Endoscopic optical coherence tomography based on a microelectromechanical mirror

Yingtian Pan

Departments of Medicine and Bioengineering, University of Pittsburgh, 3550 Terrace Street, Pittsburgh, Pennsylvania 15261, and Science and Technology Center, Carnegie Mellon University, 4400 Fifth Avenue, Pittsburgh, Pennsylvania 15213

Huikai Xie

Department of Electrical and Computer Engineering, Carnegie Mellon University, 5000 Forbes Avenue, Pittsburgh, Pennsylvania 15213

Gary K. Fedder

Department of Electrical and Computer Engineering and the Robotics Institute, Carnegie Mellon University, 5000 Forbes Avenue, Pittsburgh, Pennsylvania 15213

Received August 8, 2001

An endoscopic optical coherence tomography (OCT) system based on a microelectromechanical mirror to facilitate lateral light scanning is described. The front-view OCT scope, adapted to the instrument channel of a commercial endoscopic sheath, allows real-time cross-sectional imaging of living biological tissue via direct endoscopic visual guidance. The transverse and axial resolutions of the OCT scope are roughly 20 and 10.2 μm, respectively. Cross-sectional images of 500 $\times$ 1000 pixels covering an area of 2.9 mm $\times$ 2.8 mm can be acquired at ~5 frames/s and with nearly 100-dB dynamic range. Applications in thickness measurement and bladder tissue imaging are demonstrated.

OCIS codes: 170.2150, 170.3880, 170.4500, 170.7230, 170.3890.

Optical coherence tomography (OCT) is a newly developed optical imaging technique that permits high-resolution cross-sectional imaging of highly scattering media.[1,2] OCT is based on optical coherence-domain reflectrometry, which utilizes broadband light and interferometry to detect the path-length distribution of echoes of light from reflective interfaces. Two- and three-dimensional images can be obtained by combination of optical coherence-domain reflectrometry measurements (i.e., longitudinal scans) with sequential transverse scans. Since its initial use for imaging the transparent and low-scattering tissue of eyes,[1] OCT has become attractive for noninvasive medical imaging. It has been demonstrated[2,3] that the internal morphological and cellular structures in biological tissue are displayed by a spatially resolved map of the reflected light in an OCT image with high spatial resolution (e.g., 10 μm) and sensitivity (e.g., >100 dB). OCT imaging of a wide variety of biological tissues, and their malformations, has been reported.[2–7] Recent technological advances include real-time OCT,[2,7] ultrahigh-resolution subcellular OCT,[8] dual-wavelength and spectral OCT,[6,9] polarization OCT, and Doppler OCT to provide enhanced image contrast and diagnostic specificity.[10–12] Endoscopic OCT devices for *in vivo* imaging of internal organs have been reported, in which transverse scanning is performed either by a rotary fiber-optic joint in a circumferential pattern[2,7] or by a small galvanometric plate swinging the distal fiber tip in a line-scan pattern.[4] Nevertheless, development of high-performance, reliable, low-cost OCT catheters and endoscopes suitable for future clinical applications remains desirable.

Here we present a new endoscopic OCT system that uses a microelectromechanical system (MEMS) chip to achieve high-speed transverse light-scanning imaging in a slender endoscopic tube while maintaining high light-coupling efficiency and spatial resolution. The use of a MEMS mirror is proposed to facilitate endoscopic beam steering because of the system's small size, potentially low cost, and excellent microbeam-manipulating capacity. We describe the design and packaging of the electro-thermal MEMS mirror and present preliminary test results to show the performance of the OCT scope and its applications in tissue imaging.

A schematic of the endoscopic OCT system is shown in Fig. 1. A high-brightness, broadband light source is coupled into a fiber-optic Michelson interferometer. The pigtailed output power P of the light source is 12 mW, the central wavelength λ_0 is 1320 nm, and the FWHM spectral bandwidth $\Delta\lambda$ is 77 nm. The input light beam is divided equally into two arms of a Michelson interferometer (50%:50%). In the reference arm

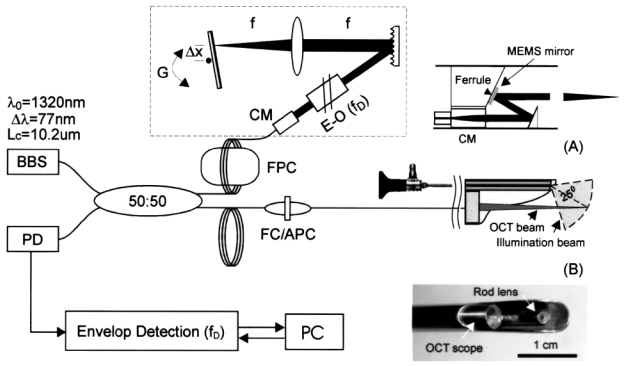

Fig. 1. Schematic of the endoscopic OCT system. Insets (A) and (B), optical arrangement and photograph of the distal OCT scope, respectively; BBS, broadband source; PD, photodiode, G, galvanometric mirror. Other abbreviations defined in text.

0146-9592/01/241966-03$15.00/0

of the fiber-optic interferometer, a fiber polarization controller (FPC) is used to ensure that the polarization of light exiting the nonpolarization-maintaining fiber is almost linearly polarized. The light from the fiber end face is coupled into a ϕ 2-mm collimated beam by an angle-polished gradient-index lens (CM) and then guided to a high-speed depth scanning unit containing an electro-optic (E-O) phase modulator and a rapid-scanning grating-lens-based optical delay line to implement OCT imaging in real time.

The principle of a grating-lens-based optical delay line was outlined previously.[2,13] This method permits phase and group delays to be independently managed. In the previously reported arrangements, the phase shift was controlled by adjustment of offset Δx of the tilting mirror, which resulted in increased mirror size and in turn restricted the speed of the depth scanning. To overcome this technical limitation, we center the galvo mirror ($\Delta x = 0$) and insert an electro-optic phase modulator to generate a higher and more-stable Doppler frequency shift for heterodyne detection. By carefully choosing the parameters of each component, we achieve a high-speed depth scanner that permits the acquisition of 2.4 K axial scans/s with an optical delay window of 2.8 mm (higher-path-length delay is possible with increasing tilting angle). The high and stable Doppler frequency shift results in an increased signal-to-noise ratio of the signal processing electronics. Moreover, we can minimize the dispersion induced by unbalanced fiber lengths and optical components between the two arms of the Michelson interferometer by slightly moving the grating along the optical axis, which can greatly enhance the axial resolution.

The fiber end in the sample arm of the interferometer is connected to a pigtailed OCT scope through a modified angle-polished fiber connector (FP/APC) connector, which can be inserted into the ϕ 4-mm instrument channel of a 22 French (Fr) endoscope. Inset (A) of Fig. 1 is a schematic of the optical arrangement in the distal OCT scope, and inset (B) is a photograph of an OCT scope. The light from the fiber is coupled into a ϕ 0.8-mm collimated beam, deflected by a pair of mirrors, and then focused by a laser doublet (f-10 mm/ϕ 5-mm) to a roughly ϕ 20-μm spot size on the image plane. The transverse light scanning in the OCT scope is facilitated by a MEMS planar mirror whose structure is shown in Fig. 2 by a scanning-electron micrograph.

The large, 1 mm $\times$ 1 mm, MEMS mirror used in this study is a single-crystalline silicon chip fabricated by a recently developed deep reactive-ion-etching Al-coated complementary metal-oxide semiconductor (CMOS)–MEMS process to ensure a large actuation range and optical grade flatness.[14] It is an electrothermally actuated microscanner whose hinge is a bimorph thermal actuator composed of a stack of Al ($t_1 = 0.7$ μm) and SiO_2 ($t_2 = 1.2$ μm) thin films. Because of residual stress and a difference in the thermal expansion coefficients between these two thin layers, the hinge curls up to an initial bending angle $\theta_0 \approx 17°$ above the chip plane, and bending angle θ changes with the temperature within the bimorph. The polysilicon thermal resistor embedded in the bimorph mesh acts as a heat source to actuate the hinge of the mirror, and the relationship between actuation angle θ and external voltage V can be approximated as[15]

$$\theta = k(E_1, E_2, t_1, t_2) L \Delta\alpha \Delta T \propto V^2, \tag{1}$$

where k is a coefficient related to Young's modulus E and to the thickness t of the two layers. L is the length of the stacked thin films; $\Delta\alpha$ is a differential thermal expansion coefficient between Al and SiO_2. The induced temperature difference ΔT is approximately related to V^2. Preliminary test results show that the resistance of the embedded polysilicon heater is 2.2 kΩ. The maximal electrical current or voltage applied to the heater is 15 mA, corresponding to 33 V. The resonant frequency of the CMOS MEMS mirror is 165 Hz, exceeding the speed requirement for most one-dimensional endoscopic laser scanning applications. According to relation (1), the scan is nonlinear, and nonlinear correction to the applied voltage is required.

Because initial bending angle is 17°, the ferrule that houses the MEMS mirror has to be tilted to roughly 17°/2 to maintain the reflected beam to the center of the optical axis. The results on a test stage show that the mechanical scan angle is of the order of $\pm 8°$, yielding a $\pm 15°$ optical scan angle for beam steering. However, because of improper angular setting of the ferrule end face in our initial packaging, the deflected beam deviates from the optical axis, and the tested maximal scan range is 2.9 mm when an $f = 10$ mm scan lens is used. The detected interferometric signal is preamplified by a low-noise, broadband transimpedance amplifier (Femto Model HCA-10M-100K), bandpass filtered, and demodulated before being digitized by a 5-MHz, 12-bit analog-to-digital converter. Both the depth scan and the lateral MEMS scan are synchronized with the image data acquisition by use of two 16-bit digital-to-analog channels.

To demonstrate the use of MEMS for endoscopic light-scanning imaging, we imaged a glass slide to verify the field flatness and biological tissues *in vivo* to show image fidelity. Figure 3 is an OCT image of the border of a 225-μm-thick cover slide stacked upon a 1-mm-thick glass plate. The 500 $\times$ 1000 pixel cross section, which covers an area of 2.9 mm $\times$ 2.8 mm, was acquired at ~5 frames/s. The results demonstrate the field flatness of an endoscopic OCT system

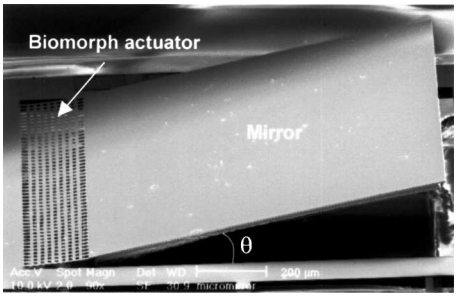

Fig. 2. Scanning-electron micrograph of the CMOS–MEMS mirror.

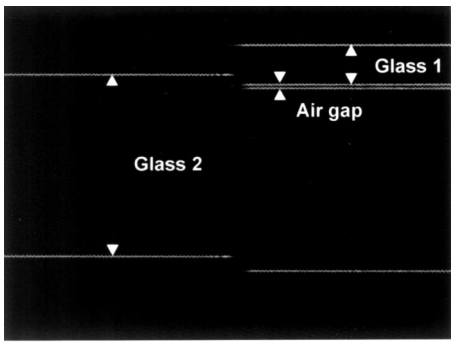

Fig. 3. Two-dimensional OCT of two stacked microscope glass slides with thicknesses of 225 μm and 1 mm.

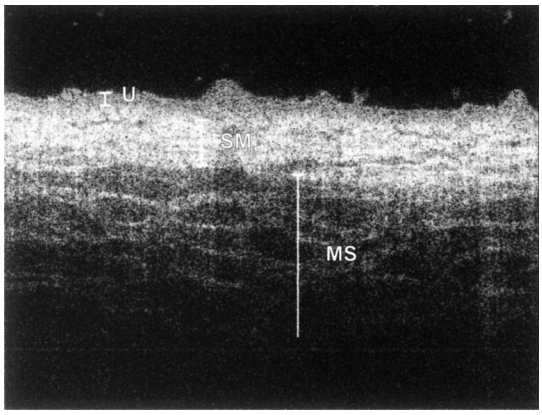

Fig. 4. *In vivo* two dimensional endoscopic OCT of porcine bladder through cystotomy: U, urothelium; SM, submucosa; MS, muscularis layer.

with a MEMS mirror for light steering in the lateral direction. Figure 4 is an OCT image of a porcine urinary bladder *in vivo*. Although the image fidelity (e.g., signal-to-noise ratio and imaging depth) is slightly less than that obtained by our nonendoscopic OCT system,[3] possibly because of higher coupling loss (>3 dB) in the OCT scope, morphological details in the bladder wall, e.g., the urothelium, the submucosa, and the upper muscularis layer are readily delineated. Because most transitional cell carcinomas originate in the urothelium, our results demonstrate the potential of MEMS-based endoscopic OCT for early detection and staging of bladder cancers. Also, as a wide variety of inner organs (e.g., cervix, colon, joints) can be imaged by front-view endoscopic OCT, the results suggest potential applications of this technique for noninvasive or minimally invasive imaging diagnosis in these tissues.

In summary, we have demonstrated a novel front-view OCT endoscope based on a CMOS MEMS mirror for endoscopic light steering to achieve biomedical imaging at transverse and axial resolutions of roughly 20 and 10 μm, respectively. Cross-sectional images of 500 $\times$ 1000 pixels covering an area of 2.9 mm $\times$ 2.8 mm can be acquired at ~5 frames/s and with a nearly 100-dB dynamic range. It should be noted that a large (ϕ 5-mm) OCT scope was chosen because it can use the entire internal clearance of a 22 Fr endoscope. Smaller OCT scopes can be developed to accommodate various types of endoscope.

This research is supported in part by National Institutes of Health contract 1-R01-DK059265-01 (with Y. Pan), by Whitaker Foundation contract 00-0149 (with Y. Pan), and by the Defense Advanced Research Projects Agency Air Force Materiel Command, U.S. Air Force, under agreement F30602-97-2-0323 (with G. Fedder). Y. Pan's e-mail address is pany@msx.dept-med.pitt.ed.

References

1. D. Huang, E. A. Swanson, C. P. Lin, J. S. Schuman, W. G. Stinson, W. Chang, M. R. Hee, T. Flotte, K. Gregory, C. A. Puliafito, and J. G. Fujimoto, Science **254,** 1178 (1991).
2. G. A. Tearney, M. E. Brenzinski, B. E. Bouma, S. A. Boppart, C. Pitris, J. F. Southern, and J. G. Fujimoto, Science **276,** 2037 (1997).
3. Y. T. Pan, J. P. Lavelle, S. Bastacky, M. Zeidel, and D. Farkas, "Detection of tumorgenesis in rat bladders with optical coherence tomography," Med. Phys. (to be published).
4. A. M. Sergeev, V. M. Gelikonov, G. V. Gelikonov, F. I. Feldchtein, R. V. Kuranov, N. D. Gladkova, N. M. Shakhova, L. B. Snopova, A. V. Shakov, I. A. Kuznetzova, A. N. Denisenko, V. V. Pochinko, Yu. P. Chumakov, and O. S. Streltzova, Opt. Express **1,** 421 (1997), http://www.opticsexpress.org.
5. J. M. Schmitt, M. Yadlowsky, and F. Bonner, Dermatology **191,** 93 (1995).
6. Y. T. Pan and D. L. Farkas, J. Biomed. Opt. **3,** 446 (1998).
7. A. M. Rollins, R. Ung, A. Chak, C. Wong, K. Kobayashi, M. V. Sivak, and J. A. Izatt, Opt. Lett. **24,** 1358 (1999).
8. W. Drexler, U. Morgner, F. X. Krtner, C. Pitris, S. A. Boppart, X. D. Li, E. P. Ippen, and J. G. Fujimoto, Opt. Lett. **24,** 1221 (1999).
9. U. Morgner, W. Drexler, F. Krtner, X. Li, C. Pitris, E. Ippen, and J. Fujimoto, Opt. Lett. **25,** 111 (2000).
10. C. Saxer, J. de Boer, B. Park, Y. Zhao, Z. Chen, and J. Nelson, Opt. Lett. **25,** 1355 (2000).
11. G. Yao and L.-H. Wang, Opt. Lett. **24,** 537 (1999).
12. S. Yazdanfar, A. M. Rollins, and J. A. Izatt, Opt. Lett. **25,** 1448 (2000).
13. G. Tearney, B. Bouma, and J. Fujimoto, Opt. Lett. **22,** 1811 (1997).
14. H. Xie, X. Zhu, L. Erdmann, K. J. Gabriel, and G. K. Fedder, in *Solid-State Sensor and Actuator Workshop* 77 (2000).
15. H. Xie, Y. Pan, and G. K. Fedder, presented at the 15th IEEE International MEMS Conference, Las Vegas, Nev., January 20–24, 2001.